BASIC RESEARCH STUDIES

Particle hemodynamics analysis of Miller cuff arterial anastomosis

P. Worth Longest, PhD, Clement Kleinstreuer, PhD, and **Joseph P. Archie, Jr, PhD, MD,** *Raleigh, NC*

Objective: Studies of animal and human below-knee anastomoses with Miller cuffs indicate that improved graft patency results from redistribution of intimal hyperplasia away from areas critical to flow delivery, such as the arterial toe. We hypothesize that particle hemodynamic conditions are a biophysical mechanism potentially responsible for the clinically observed shift in intimal hyperplasia localization associated with better patency of the Miller configuration.

Methods: Computational fluid dynamics analysis of vortical flow patterns, wall shear stress fields, and potential for platelet interaction with the vascular surface was performed for realistic three-dimensional conventional and Miller cuff distal end-to-side anastomoses. Sites of significant platelet-wall interaction, including elevated near-wall particle concentrations and stasis, were identified with a validated near-wall residence time model, which includes shear stress–based factors for particle activation and surface reactivity.

Results: Particle hemodynamics largely coincide with the observed redistribution of intimal hyperplasia away from the critical arterial toe region. Detrimental changes in wall shear stress vector magnitude and direction are significantly reduced along the arterial suture line of the Miller cuff, largely as a result of increased anastomotic area available for flow redirection. However, because of strong particle-wall interaction, resulting high near-wall residence time contours indicate significant intimal hyperplasia along the graft-vein suture line and in the vicinity of the arterial heel.

Conclusions: While a number of interacting mechanical, biophysical, and technical factors may be responsible for improved Miller cuff patency, our results imply that particle hemodynamics conditions engendered by Miller cuff geometry provide a mechanism that may account for redistribution of intimal hyperplasia. In particular, it appears that a focal region of significant particle-wall interaction at the arterial toe is substantially reduced with the Miller cuff configuration. (J Vasc Surg 2003;38:1353-62.)

Clinical Relevance: The search continues for distal anastomotic geometries of synthetic bypass grafts that result in improved patency rates equal to or better than those obtainable with saphenous vein grafts. Using computational fluid particle dynamics analysis of a three-dimensional realistic Miller cuff distal anastomosis, we found that the Miller cuff redistributes adverse particle hemodynamics, attributed to intimal hyperplasia and graft failure, away from the anastomotic toe, a common point of failure. These results explain in part the clinical observations of improved patency of Miller cuffed grafts. Computational analysis of vascular disorders, such as arterial stenosis, bypass graft placement, graft failure, and aneurysm formation and rupture, enables significant advances in providing quantitative guidance for surgical interventions and clinical management.

Occlusion of synthetic peripheral bypass grafts is frequently caused by intimal hyperplasia or thrombosis at the distal anastomosis. For below-knee distal anastomoses, clinical evidence indicates that interpositioned vein cuffs[1,2] and vein patches[3] substantially extend graft function. A number of potential surgical, hemodynamic, and biologic mechanisms have been associated with improved patency of vein-supplemented designs[2,4-6]; however, the relative significance of these factors has not been determined.

Regarding the Miller cuff, Stonebridge et al[2] found no improvement in patency associated with distally cuffed above-knee polytetrafluoroethylene (PTFE) popliteal artery bypass grafts. However, patency rate was significantly improved for below-knee popliteal artery PTFE bypass grafts with a Miller cuff, compared with standard end-to-side anastomoses. Qualitative angiograms and pathologic studies with Miller-style grafts in human beings[7] and animals[6,8] indicate that a potential mechanism for improved graft performance is redistribution of distal anastomotic intimal hyperplasia away from critical areas, such as the arterial heel, toe, and floor. Most significant intimal hyperplasia was observed at the graft-cuff interface of the Miller design, where it is better accommodated by the larger cross-sectional area. The observed shift in intimal hyperplasia occurrence is particularly significant, considering the
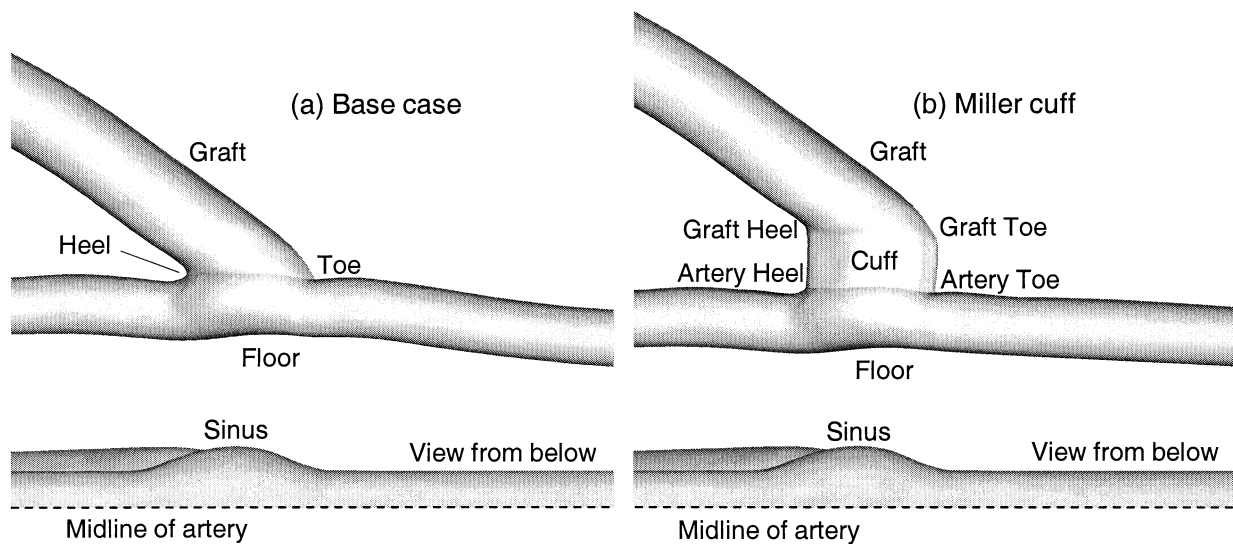
Fig 1. Geometric surface models of distal end-to-side anastomosis resulting from straight 45-degree graft-cut (base case; **a**) and similar Miller cuff configuration (**b**). Graft diameters are 6 mm; artery diameters are 4 mm; cuff height is 4 mm.

smaller arterial diameter associated with below-knee procedures, and may account for the improved patency rate reported for cuffed geometries at this location.

Hemodynamic and blood particle interaction with the vascular surface, as well as surgical injury, are inciting mechanisms capable of eliciting various cellular responses that potentially result in intimal hyperplasia. Comparisons with generalized[9] and system-specific[10,11] regions of intimal hyperplasia localization have implicated low and oscillatory shear,[10-14] as well as variations in mean wall shear stress (WSS) magnitude[15,16] and direction.[17] Intimal hyperplasia along the suture line is widely associated with surgical injury, suture technique, compliance mismatch, and intramural strain.[6,12] As with atherosclerosis, long near-wall residence time (NWRT) and deposition of critical blood particles have been associated with general qualitative sites of intimal hyperplasia development.[9,12,18]

Biophysical and computational studies of the Miller cuff have suggested that elevated wall stress, reduced compliance mismatch, and the biologic effect of a natural "buffer zone" may account for the reported higher long-term success rate with the vein-supplemented design.[4,6,8,19] Noori et al[5] and Harris and How[4] suggest that vortical flow engendered by the Miller configuration provides a beneficial "continuous washout" of the cuff cavity and augments WSS along the arterial floor. However, the hemodynamic and mechanical advantages of the Miller cuff have been widely questioned. Cole et al[20] found that aspects of the anastomotic hemodynamics were "worsened" with the cuffed configuration. Kissin et al[8] demonstrated considerably more intimal hyperplasia in a PTFE-cuffed anastomosis compared with a vein cuff, which indicates that anastomotic hemodynamics may not be responsible for the improved clinical performance of the

Miller configuration. Whereas Leuprecht et al[6] suggested that compliance mismatch was responsible for the observed shift in intimal hyperplasia formation, Norberto et al[21] found no difference in intimal hyperplasia between vein cuffs and cuffs with altered compliance. These controversial observations result in the conjecture that the beneficial effect of cuffed anastomoses below the knee is not necessarily hemodynamic or biomechanical.

In this study, the potential role of vascular hemodynamics in local development of intimal hyperplasia is further investigated, recalling that both a locally dysfunctional endothelium and excessive blood particle depositions are precursors for intimal hyperplasia development. Specifically, it is hypothesized that particle hemodynamic conditions, determined in part by anastomotic geometry, provide a biophysical mechanism that is potentially responsible for the clinically observed shift in intimal hyperplasia localization and associated improved patency of the Miller cuff. Numerical simulations were performed to compare the vascular hemodynamics of conventional and Miller-style anastomotic configurations in terms of velocity fields and selected particle trajectories. Assuming comparable compliance among grafts, we assessed the potential for intimal hyperplasia, on the basis of wall hemodynamics, including a NWRT model[22] for platelet interaction with the vascular surface.

METHODS

To construct a realistic femoropopliteal distal anastomosis,[23] a thin-walled 6-mm PTFE graft (Impra Bard, Tempe, Ariz) was pressed flat and cut at an approximate 45-degree angle. The graft was then sutured end-to-side to a 4-mm thin-walled PTFE graft, which represented the recipient artery. The anastomosis was filled with RTV poly-
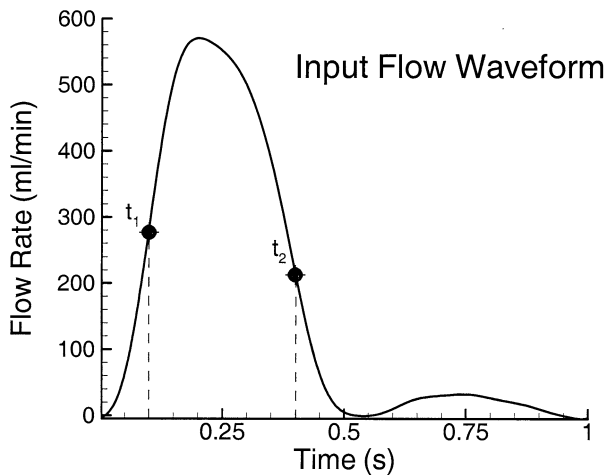
Fig 2. Standard type I input pulse for a 6-mm graft consistent with typical postsurgical observations of human femoropopliteal bypass graft. Mean flow rate is 166 mL/min.

urethane rubber (Poly 74-30; Polytek, Easton, Pa) to a static pressure of 100 mm Hg, and was cured. An internal cast of the graft was excised and digitized with three-dimensional laser scanning (First Article Corp, New Hope, Minn). The resulting conventional or base case anastomotic geometry is illustrated in Fig 1, *A.* Similarly, a 4-mm-wide strip of PTFE was situated between the graft and artery to represent the venous cuff of the Miller configuration, as shown in Fig 1, *B.* Surface models were constructed to maintain key geometric features, such as graft and artery cross-sectional variations from construction of the anastomosis. In both configurations, opening of the artery in the region of the anastomosis induced an elliptical arterial cross section and a raised vessel floor, as seen in actual cases. A gently curving inlet graft section, as observed in vivo by Bertschinger et al,[24] was assumed, and was consistently applied to both models. The vessel walls were assumed rigid and symmetric about an axial centerline plane.

A transient type I input pulse, consistent with postsurgical observations of femoral bypass grafts, has been implemented for both graft geometries, and is shown in Fig 2.[23] The input pulse selected is well within the range of typical mean flow rate for 6-mm femoral bypass grafts, and falls within peak velocity and Reynolds number guidelines for nonstenosed grafts.[25,26] A distal-to-proximal outflow ratio of 80:20 was assumed for all cases.

Flow field equations describing laminar incompressible hemodynamics include conservation of mass and momentum, as described in Kleinstreuer and Longest.[27] A transformed Quemada[28] model was used to account for the variable viscosity of blood, which can significantly affect hemodynamic conditions within critical low shear regions and during periods of flow reversal.[29] The computational software package CFX 4.4 (ANSYS, Canonsburg, Pa), which is a finite-volume code that implements multiblock

structured meshes, was used to solve flow field equations. This commercial package is supplemented with our own user-supplied Fortran programs for calculation of shear rate–dependent blood viscosity, input profiles, flow field solution convergence, transient particle tracking, and post-processing.[27] Solution convergence and grid independence of all numerical results has been verified.[23] Flow field validation for particle hemodynamic systems was achieved with comparisons to multiple in vitro results.[30,31]

Hemodynamic parameters encapsulating disturbed flow interaction with the vessel wall include the magnitude of the time-averaged WSS, wall shear stress gradient (WSSG), wall shear stress angle gradient (WSSAG), and oscillatory shear index (OSI). The detailed evaluation and biological relevance of these and other hemodynamic parameters are discussed in Kleinstreuer et al[17] and in numerous studies cited therein.

One-way coupled trajectories of critical blood particles, such as platelets (particle diameter $d_p \approx 4$ μm), were calculated on a lagrangian basis by integrating an appropriate version of the particle trajectory equation within three-dimensional transient non-newtonian fluid flow fields. Terms for Stokes drag, the near-wall drag modification, or the "lubrication" force, the pressure gradient, and near-wall lift, were included in the simulation of blood particle motion.[23,30] Red blood cell–induced platelet dispersion was accounted for by incorporating an appropriate diffusivity approximation.[32] Particle trajectories were calculated as a postprocessing step, with an adaptive step-size controlled integration scheme, as described by Longest et al.[30]

Regions of significant platelet interaction with the vascular surface were identified by NWRT, which has been formulated to quantify particle stasis and elevated near-wall concentrations on a nondimensional basis.[22,23] The NWRT concept is an approximate method that is particularly useful and necessary, given that factors such as vessel surface roughness, actual blood particle shape, and nanoscale bond formations responsible for possible cell attachment, rolling, or resuspension cannot feasibly be included in simulations involving relatively large-scale geometries. For calculation of NWRT, at least 500,000 blood particles were released randomly in both space and time over one pulse period at an upstream section before the junction region. The simulations were continued until all particles exited the flow field. NWRT has been validated by comparison with measured deposition data in uniformly reactive axisymmetric geometries[22,23] and monocyte depositions in a rabbit aortoceliac model.[33] To address the effects of platelet activation and variable wall reactivity, a composite nondimensional model for platelet-wall interaction has been formulated, as outlined in Fig 3 and discussed in the following paragraphs.

To account for platelet activation, it is assumed that shear stress exposure sensitizes platelets to many chemical agonists[34] and that a spectrum of platelet activation may occur.[35] Mechanical factors that affect platelet activation include the level of shear stress to which a platelet is
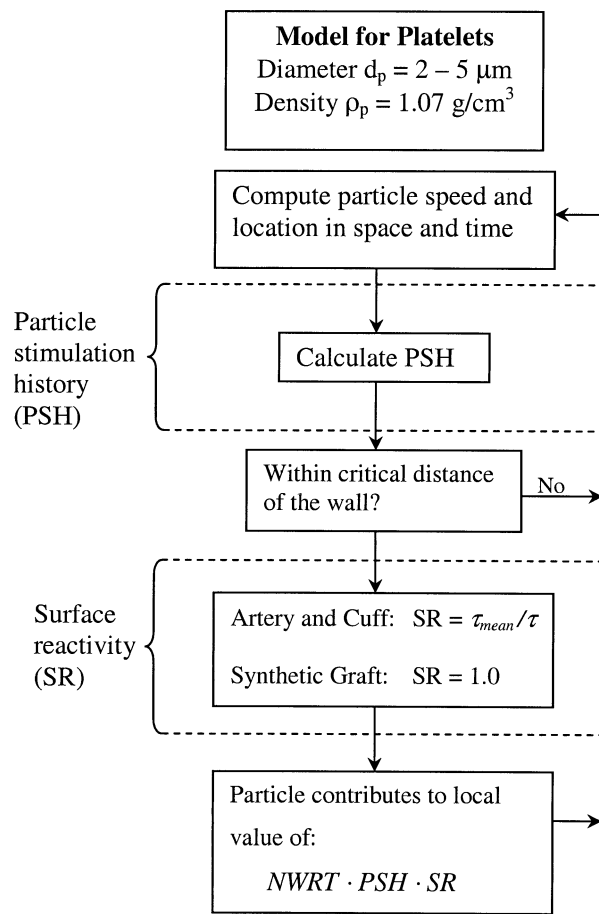
```
┌─────────────────────────────────┐
│        Model for Platelets       │
│   Diameter dₚ = 2 – 5 μm         │
│   Density ρₚ = 1.07 g/cm³        │
└─────────────────────────────────┘
```

Model for Platelets
Diameter $d_p = 2 - 5$ μm
Density $\rho_p = 1.07$ g/cm^3

Compute particle speed and location in space and time

Particle stimulation history (PSH)

Calculate PSH

Within critical distance of the wall? → No

Surface reactivity (SR)

Artery and Cuff: $SR = \tau_{mean}/\tau$

Synthetic Graft: $SR = 1.0$

Particle contributes to local value of:

$$NWRT \cdot PSH \cdot SR$$

Fig 3. Outline of composite near-wall residence time *(NWRT)* model for platelets, including platelet stimulation history *(PSH)* and wall shear stress–based surface reactivity *(SR)* factors. All parameters are nondimensional.

subjected and the exposure time,[35] as encapsulated by the platelet stimulation history.[23]

When present, endothelial cells are capable of synthesizing and expressing procoagulate and anticoagulate proteins, which regulate adhesion of platelets to the vascular surface. Endothelial cell–derived antithrombogenic compounds include prostacyclin (prostaglandin 2 [PGI_2]), nitric oxide, and tissue factor pathway inhibitor.[36] Endothelial cells produce antithrombogenic proteins to counteract thrombogenic tissue factor production, which occurs in areas of endothelial dysfunction, activation, and injury.[37] A direct relationship has been identified between local endothelial cell exposure to WSS and expression of antithrombogenic compounds, including PGI_2, nitric oxide, and tissue factor pathway inhibitor.[37,38] Therefore platelet interaction with an intact but potentially dysfunctional or injured endothelium are mitigated in regions of high WSS. It is hypothesized that regions of high and low WSS (τ_w) are relatively proportional to the mean WSS of the vessel (τ_{mean}). A surface reactivity (SR) factor to quantify the local

significance of platelet interaction with an intact endothelium is defined as $SR = \tau_{mean}/\tau_w$, which is based on the potential for adhesion in the presence of coagulate and anticoagulate proteins.[23] For a 4-mm popliteal or tibial artery and the applied inlet conditions, a standard value of $\tau_{mean} = 14$ dyne/cm^2 has been assumed.

To account for the interdependent effects of platelet-wall interaction, a composite parameter is needed that includes platelet activation (platelet stimulation history) and surface reactivity as part of the NWRT model. Thus we hypothesize that unactivated platelets or endothelium expression of antithrombogenic compounds may largely eliminate the hyperplastic effect of platelet-wall interaction. In contrast, activated platelets and a reactive (or thrombogenic) surface most likely enhance the potential for intimal hyperplasia arising from platelet-wall interaction. Therefore we have proposed a parameter in which the surface reactivity (SR) and platelet stimulation history (PSH) factors are used to scale local NWRT, that is, $NWRT \cdot PSH \cdot \cdot SR$.[39] Calculation of this composite NWRT is outlined in Fig 3. It is noted that of these parameters only surface reactivity captures low WSS effects. In contrast, the platelet stimulation history function is increased by high shear stress exposure over the lifetime of the platelet. Furthermore, regions of significant near-wall particle concentrations, as determined by convection and diffusion of discrete elements, do not directly coincide with local WSS conditions.[22,23]

RESULTS

Anastomotic hemodynamics. Velocity profiles and secondary streamlines for the conventional (base case) and Miller cuff anastomoses are given in Fig 4. Due to the non-newtonian shear-thinning viscosity of blood, a relatively blunt velocity profile is observed in the graft of the base case model during systolic flow acceleration (t_1; Fig 4, *A*). Furthermore, minimal flow separation is observed in the vicinity of the toe, resulting in the relatively weak secondary flow noted at section B of Fig 4, *A*. In the Miller cuff anastomosis during flow acceleration (t_1; Fig 4, *B*), a relatively large area is available for flow redirection, which well accommodates flow reversal associated with proximal outflow. As a result of enhanced lateral momentum transport arising from the increased viscosity of the low shear cuff region, midplane recirculation is not apparent at time t_1. Separation is observed in the toe region, resulting in a significant axial vortex, evident at section B in Fig 4, *B*. However, the underlying axial velocity in the region of the vortex is relatively high; thus reduced particle-wall interaction can be expected from this secondary mechanism.

As a result of inlet curvature, the upstream velocity profiles entering the base case and Miller cuff geometries at time t_2 are skewed toward the upper graft surface (Fig 4, *C*, *D*). As a result of flow separation in the region of the toe, a significant recirculation bubble extends downstream, and is most pronounced for the Miller cuff. This separation is characterized by a region of low pressure; thus a circumferential pressure gradient arises. The interaction of the downward inertia of the central fluid core, coupled with the
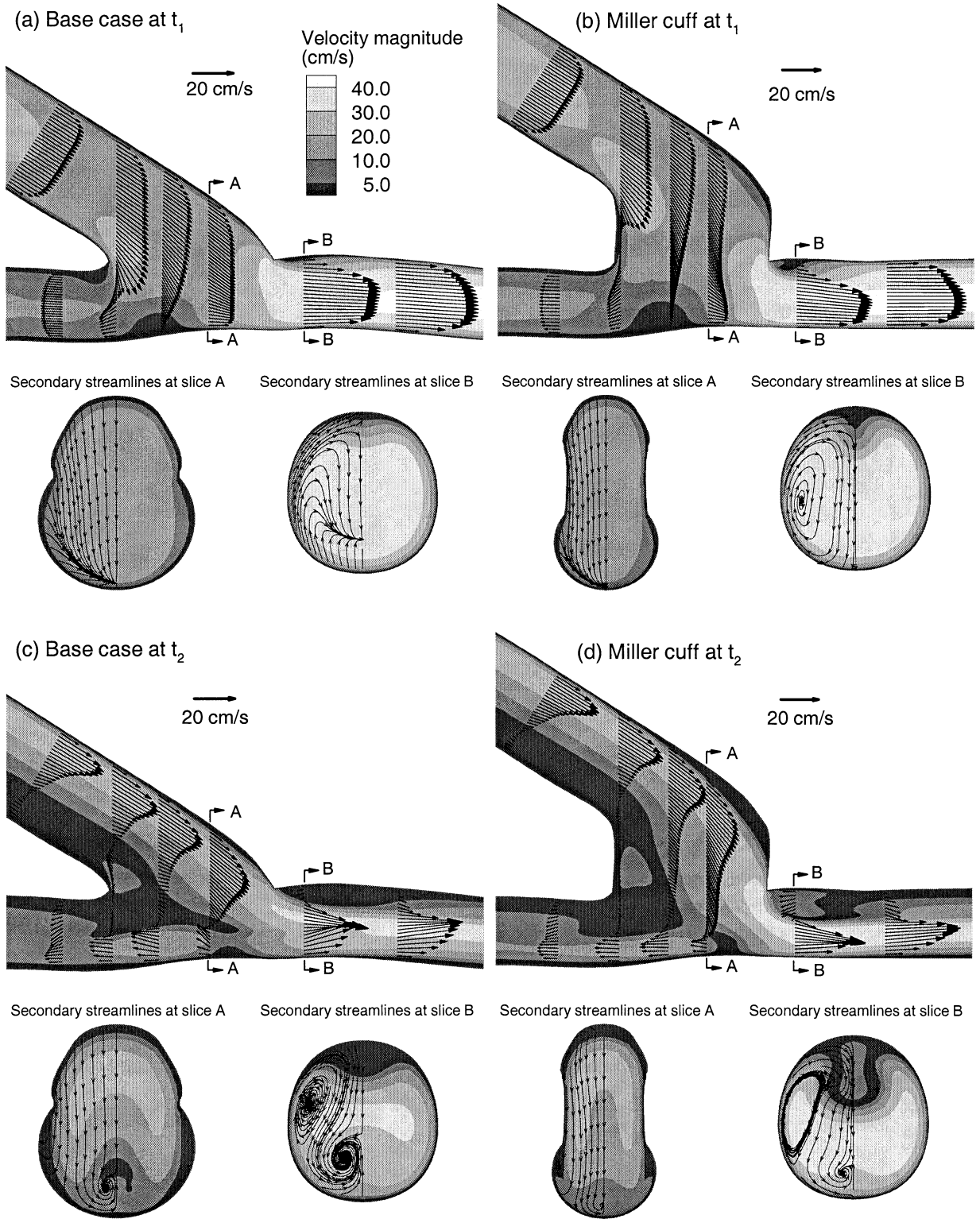
Fig 4. Midplane velocity vectors, contours of velocity magnitude, and streamlines of secondary motion for base case (**a, c**) and Miller cuff (**b, d**) during accelerating (t_1; **a, b**) and decelerating flow (t_2; **c, d**). Cross-sections scaled to highlight vortical flow features.

existence of a circumferential pressure gradient, results in a set of mid-plane symmetric vortices, shown to rotate clockwise in section B of the base case and Miller cuff (Fig 4, *C, D*) during flow deceleration (t_2). While the occurrence of significant secondary vortices enhances the transport of centralized fluid elements toward the vascular wall, coinciding regions of elevated axial flow are expected to reduce this effect. As a result of flow division, regions of vortical recirculation are observed in the midplane, near the heels of both configurations, and extend proximally within the graft lumen at time t_2 (Fig 4, *C, D*). While this midplane vortical pattern appears similar in both configurations, it is more pronounced and remains active during a longer portion of the flow cycle in the Miller cuff. In comparison with the base case, velocity magnitude in the midplane is significantly higher in the immediate region of the Miller cuff suture line toe, particularly for time t_2.

WSS-based hemodynamics. Surface contours of WSS, OSI, WSSG, and WSSAG for the base case and Miller cuff anastomoses are shown in Fig 5. For the base case, the midfloor region and lateral sinus wall are characterized by low WSS and high OSI, which indicate potential intimal hyperplasia (Fig 5, *A, C*). The anastomotic toe in the vicinity of the suture line displays high WSS and low OSI; however, a region just distal to the toe presents WSS conditions potentially conducive to intimal hyperplasia. Regions of low WSS and high OSI in the Miller cuff are observed at the distal graft-vein junction and the proximal vein-artery junction (Fig 5, *B, D*). However, a protective region of relatively high WSS and low OSI is observed along the cuff, which appears to be the primary route of flow delivery. In comparison with the base case, WSS is approximately 10% higher in the midfloor region of the Miller cuff configuration (Fig 5, *A, B*).

Changes in mean WSS magnitude and direction, as quantified by WSSG and WSSAG, are most pronounced along the suture line of the base case, with elevated contours occurring at the toe and heel (Fig 5, *E, G*). Significant contours of the WSSG and WSSAG also encompass the sinus region and extend to the arterial floor. In the Miller configuration, contours of the WSSG and WSSAG are moderately reduced along the vein-artery interface, in comparison with the base case (Fig 5, *E-H*). The Miller cuff apparently distributes changes in wall shear stress vector magnitude and direction over a broader region, resulting in elevated contours at the graft-vein interface. Furthermore, WSSG and WSSAG contours at the mid-arterial floor appear moderately elevated (10%) for the Miller cuff in comparison with the base case.

Near-wall residence time model. Convergent profiles of composite near-wall residence time, based on 500,000 platelet trajectories, indicate significant particle-wall interaction along the suture line of the base case configuration, particularly at the toe, heel, and mid-suture line (Fig 6, *A*). As a result of significant particle recirculation and low WSS, elevated NWRT is also observed in the sinus region of the base case configuration, with moderate contours extending to the arterial floor. In the Miller cuff

configuration, NWRT predicts high platelet-wall interaction along the graft-vein suture line and in the immediate region of the heel (Fig 6, *B*). The focal region of elevated NWRT just proximal to the arterial toe of the base case is largely reduced with construction of the cuff (Fig 6). Specifically, the maximum composite NWRT in the arterial toe region of the base case is 28.7 (nondimensional), compared with a maximum arterial toe value of 2.6 for the Miller cuff. However, particle-wall interaction appears similar for both configurations in the sinus or lateral wall region and along the arterial floor.

The relative potential for platelet-wall interaction within broad regions of each configuration, as estimated by area-averaged values of NWRT, are given in Fig 7. Area-averaging was performed within a region that extends approximately 8 mm from the suture line along each anastomotic branch. Circumferential quadrants of the artery and graft were used as regional boundaries for the toe, heel, floor, and lateral wall. For the Miller cuff, an additional boundary was defined midway the cuff height to specify graft and artery side components of the toe and heel. Extensions of these boundaries did not significantly affect the proportional relationship of the area-averaged values. In comparison with the base case toe region, a moderately reduced area-averaged value of the composite NWRT is observed for the Miller cuff at the graft toe; however, a considerable reduction is observed for the arterial toe of the Miller cuff. The area-averaged contours indicate potentially aggressive intimal hyperplasia at the arterial heel of the Miller cuff, whereas the graft heel region is expected to be relatively spared. Compared with the high NWRT in the proximal arterial floor segment of the base case, area-averaged NWRT are moderately lower for the floor of the Miller cuff. Furthermore, area-averaged NWRT appear similar for the lateral walls of both configurations.

DISCUSSION

Numerical simulations were conducted to assess the particle hemodynamic characteristics and related potential for intimal hyperplasia in conventional (ie, base case) and Miller-style configurations. A number of hemodynamic or blood element interactions with the vascular surface have been directly associated with smooth muscle cell migration, proliferation, and synthesis of extracellular matrix, which characterize intimal hyperplasia. Persuasive evidence suggests that multiple endothelial responses to low WSS conditions are capable of eliciting intimal hyperplasia,[36,40] in the absence of particle-wall interaction. An endothelial shape or signaling response, capable of producing intimal hyperplasia, has been related to the gradients of the time-averaged WSS magnitude (WSSG) and direction (WSSAG).[17,41-44] It is proposed that signaling responses arising within focal regions of significantly elevated WSSG and WSSAG dominate the regulatory nature of the endothelium, resulting in spatially corresponding intimal hyperplasia. Cellular level links between aggressive intimal hyperplasia and platelet-wall interaction include release of chemotactic and mitogenic growth factors, such as platelet-
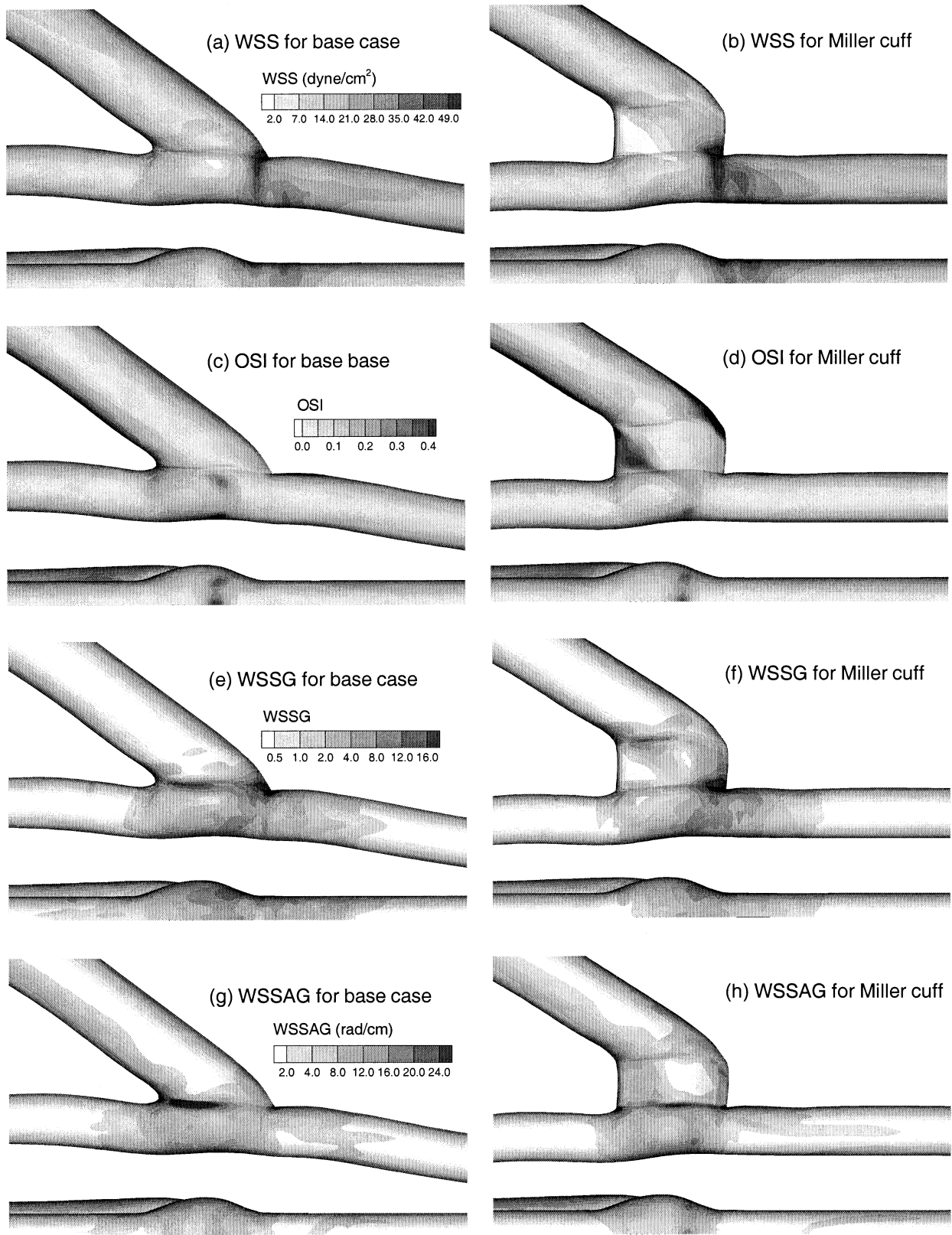
Fig 5. Wall shear stress *(WSS)*, oscillatory shear index *(OSI)*, wall shear stress gradient *(WSSG)*, and wall shear stress angle gradient *(WSSAG)* for base case (**a, c, e, g**) and Miller cuff (**b, d, f, h**) anastomoses.
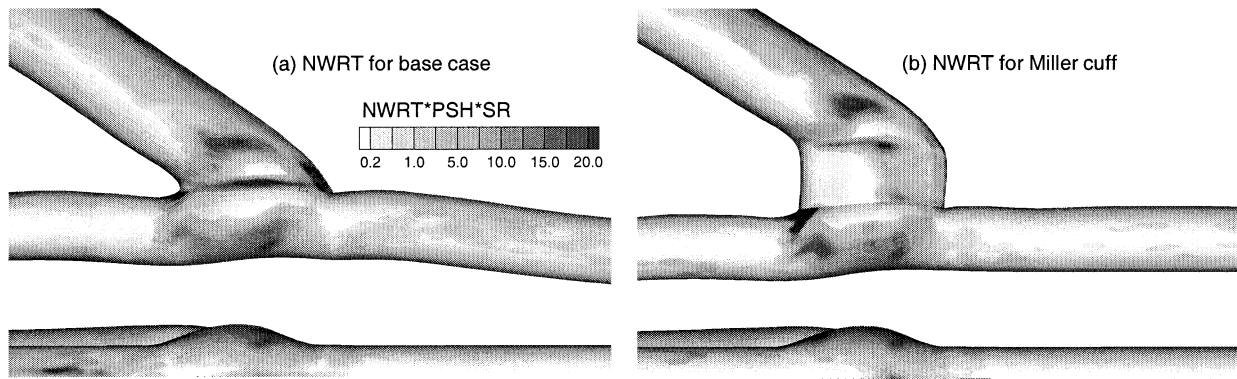
Fig 6. Near-wall residence time *(NWRT)* contours for platelet trajectories in base case **(a)** and Miller cuff **(b)**, including platelet stimulation history *(PSH)* and surface reactivity *(SR)* conditions.
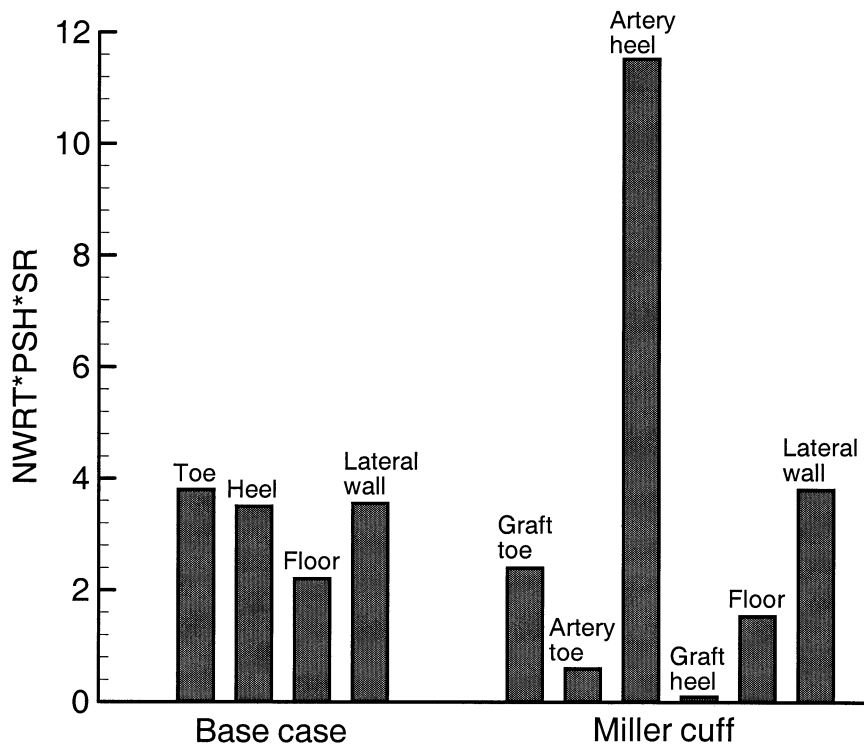

Fig 7. Area-averaged near-wall residence time *(NWRT)*, including platelet stimulation history *(PSH)* and surface reactivity *(SR)* for critical junction regions.

derived growth factor, and vascular constrictive agents, such as thromboxane A_2.[45] Permanent adhesion of platelets to the vascular surface may not be necessary for significant promotion of intimal hyperplasia.[46] Alternatively, mural thrombi resulting from significant platelet adhesion and aggregation may evolve into active atherosclerotic plaquelike lesions,[47] particularly on synthetic surfaces.[48] Factors such as compliance mismatch, intramural stress and strain, and surgical injury were not directly assessed in this study.

Previous experimental and numerical analyses of anastomotic designs have focused on associations between intimal hyperplasia and disturbed flow characteristics in the junction region, including coherent vortices,[4] regions of low WSS,[19] and significant changes in WSS vector direction and magnitude, as quantified by WSSG, WSSAG, and OSI.[15,31,49] Studies that compared conventional and Miller cuff anastomoses found marginal (approximately 10%) and often conflicting differences in WSS values and the derived spatial and temporal variations.[6,19,20] How-

ever, a significant biophysical role has been established for critical blood particles, such as monocytes and platelets, in initialization and progression of intimal hyperplasia. For example, interaction of activated platelets with a reactive vascular surface qualitatively correlate with system-specific observations of intimal hyperplasia.[9] In this study, sites of significant particle-wall interaction have been quantified by a composite NWRT model,[39] which includes shear stress–based factors for platelet activation as well as endothelial cell expression of antithrombogenic compounds.

On the basis of validated numerical simulations, the current results indicate favorable redistribution of adverse particle hemodynamic conditions away from the arterial toe and lateral arterial suture line of the Miller cuff. This shift in potential intimal hyperplasia localization is consistent with in vivo evidence that indicates predominate intimal hyperplasia at the graft-vein interface, where it is better accommodated by larger cross-sectional areas.[6-8] Specifically, changes in the WSS vector magnitude and direction, represented by WSSG and WSSAG, are largely reduced along the lateral arterial suture line of the Miller cuff, which is a result of the increased anastomotic area available for flow redirection. Consequently, WSSG and WSSAG are moderately elevated along the Miller cuff graft-vein anastomosis. Considering the potential influence of particle-wall interaction, NWRT contours indicate significant intimal hyperplasia along the graft-vein suture line and in the vicinity of the arterial heel. However, the potential for intimal hyperplasia is reduced at the Miller cuff toe, particularly in a focal region near the arterial suture line. In comparison with the base case, this reduction in particle interaction with the vascular surface results from higher velocity in the immediate arterial toe region of the Miller cuff. While the arterial toe is exposed to high concentrations of particles in both configurations, elevated local velocities induced by the Miller cuff design reduce the time available for biophysical particle-wall interaction, as indicated by NWRT. In contrast, lower velocity, enhanced secondary motion, and persistent vortex formation result in elevated near-wall particle stasis and increased potential for intimal hyperplasia at the arterial heel of the Miller cuff. Furthermore, increased WSS and reduced NWRT suggest a moderate reduction in potential for intimal hyperplasia along the arterial floor of the Miller cuff, which has been observed in vivo.[6] Other studies have attributed increased WSS along the arterial floor to enhanced midplane vortices engendered by the Miller cuff.[4,19] However, including the effect of variable blood viscosity indicates that the downward-oriented flow of the Miller cuff is primarily responsible for elevated flow rate and increased WSS in the immediate region of the arterial floor.

Primary limitations of the computational analysis include the assumption of rigid walls and in-plane geometries, and consideration of only one graft–artery diameter ratio. Wall compliance and out-of-plane vessel curvature may reduce near-wall particle stasis, particularly in the expanded sinus region. Although NWRT has been validated,[22,33,39] the relative weight of the included surface reactivity and platelet activation scaling factors are not known.

Furthermore, the relative responses of the primary cell types composing the various forms of graft and artery intimal hyperplasia should be considered, as well as the highly increased transient thrombogenicity of the suture line.

In conclusion, a number of mechanical, biophysical, and technical factors may be responsible for the improved patency rates observed with Miller cuff anastomoses positioned below the knee. Results of this study indicate that particle hemodynamic conditions engendered by the Miller cuff configuration provide a potential mechanism that may be partially responsible for redistribution of intimal hyperplasia away from the toe and lateral arterial suture line. In particular, it appears that a focal region of significant particle-wall interaction in the immediate vicinity of the arterial toe is largely reduced with the Miller configuration. Platelet interaction with the vessel wall was quantified with a validated NWRT, which accounts for particle stasis, elevated near-wall concentration, platelet activation, and surface reactivity. Whereas particle hemodynamic conditions indicate a potential intimal hyperplasia shift for the unique configuration of the Miller cuff, the underlying hemodynamic mechanisms responsible for this observation, such as elevated velocity in the immediate toe region, will most likely not occur in hooded distal anastomotic configurations. Therefore, these results cannot be extrapolated to predict the particle hemodynamic potential for intimal hyperplasia in commercial prosthetic PTFE grafts with pre-configured hoods. Thus, additional geometry-specific numerical simulations are warranted.

REFERENCES

1. Miller JH, Foreman RK, Ferguson L, Fads I. Interposition vein cuff for anastomosis of prosthesis to small artery. Aust N Z J Surg 1984;54:283-5.
2. Stonebridge PA, Prescott RJ, Ruckley CV. Randomized trial comparing infrainguinal polytetrafluoroethylene bypass grafting with and without vein interposition cuff at the distal anastomosis. J Vasc Surg 1997;26:543-5.
3. Taylor RS, Loh A, McFarland RJ, Cox M, Chester IF. Improved technique for polytetrafluoroethylene bypass grafting: long-term results using anastomotic vein patches. Br J Surg 1992;79:348-54.
4. Harris PL, How TV. Haemodynamics of cuffed arterial anastomoses. Crit Ischemia 1999;9:20-6.
5. Noori N, Scherer R, Perktold K, Czerny M, Karner G, Trubel W, et al. Blood flow in distal end-to-side anastomoses with PTFE and a venous patch: results of an in vitro flow visualization study. Eur J Endovasc Surg 1999;18:191-200.
6. Leuprecht A, Perktold K, Prosi M, Berk T, Trubel W, Schima H. Numerical study of hemodynamics and wall mechanics in distal end-to-side anastomoses of bypass grafts. J Biomech 2002;35:225-36.
7. Tyrrell MR, Wolfe JHN. Myointimal hyperplasia in vein collars for ePTFE grafts. Eur J Vasc Endovasc Surg 1997;14:33-6.

8. Kissin M, Kansal N, Pappas PJ, DeFouw DO, Duran WN, Hobson RW. Vein interpositioned cuffs decrease the intimal hyperplastic response of polytetrafluoroethylene bypass grafts. J Vasc Surg 2000;31:69-83.

9. Sottiurai VS. Distal anastomotic intimal hyperplasia: histocytomorphology, pathophysiology, etiology, and prevention. Int J Angiol 1999;8:1-10.

10. Keynton RS, Evancho MM, Sims RL, Rodway NV, Gobin A, Rittgers SE. Intimal hyperplasia and wall shear in arterial bypass graft distal anatomoses: an in vivo model study. J Biomech Eng 2001;123:464-73.

11. Loth F, Jones S, Zarins CK, Giddens DP, Nassar RF, Glagov S, et al. Relative contribution of wall shear stress and injury in experimental intimal thickening at PTFE end-to-side arterial anastomoses. J Biomech Eng 2002;124:44-51.

12. Bassiouny HS, White S, Glagov S, Choi E, Giddens DP, Zarins CK. Anastomotic intimal hyperplasia: mechanical injury or flow induced. J Vasc Surg 1992;15:708-17.

13. Ojha M, Ethier CR, Johnston KW, Cobbold RSC. Steady and pulsatile flow fields in an end-to-side arterial anastomosis model. J Vasc Surg 1990;12:747-53.

14. Keynton RS, Rittgers SE, Shu MCS. The effect of angle and flow rate upon hemodynamics in distal vascular graft anastomoses: an in vitro model study. J Biomech Eng 1991;113:458-63.

15. Lei M, Kleinstreuer C, Archie JP. Geometric design improvements for femoral graft-artery junctions mitigating restenosis. J Biomech 1996; 29:1605-14.

16. Steinman DA, Vinh B, Ethier CR, Ojha M, Cobbold RSC, Johnston KW. A numerical simulation of flow in a two-dimensional end-to-side anastomosis model. J Biomech Eng 1993;114:112-8.

17. Kleinstreuer C, Hyun S, Buchanan JR, Longest PW, Archie JP, Truskey GA. Hemodynamic parameters and early intimal thickening in branching blood vessels. Crit Rev Biomed Eng 2001;29:1-64.

18. White SS, Zarins CK, Giddens DP, Bassiouny H, Loth F, Jones SA, et al. Hemodynamic patterns in two models of end-to-side vascular graft anastomoses: effects of pulsatility, flow division, Reynolds number, and hood length. J Biomech Eng 1993;115:104-11.

19. How TV, Rowe CS, Gilling-Smith GL, Harris L. Interposition vein cuff anastomosis alters wall shear stress distribution in the recipient artery. J Vasc Surg 2000;31:1008-17.

20. Cole JS, Watterson JK, O'Reilly MJG. Is there a haemodynamic advantage associated with cuffed arterial anastomoses? J Biomech 2002;35: 1337-46.

21. Norberto JJ, Sidawy AN, Trad KS, Jones BA, Neville RF, Najjar SF, et al. The protective effect of vein cuffed anastomoses is not mechanical in origin. J Vasc Surg 1995;21:558-66.

22. Longest PW, Kleinstreuer C. Comparison of blood particle deposition models for non-parallel flow domains. J Biomech 2003;36:421-30.

23. Longest PW. Computational analysis of transient particle hemodynamics with applications to femoral bypass graft designs [doctoral dissertation]. Raleigh, NC: Mechanical and Aerospace Engineering Department, North Carolina State University; 2002.

24. Bertschinger K, Cassina PC, Debatin JF, Ruehm SG. Surveillance of peripheral arterial bypass grafts with three-dimensional MR angiography. Am J Roentgenol 2001;176:215-20.

25. Nielsen TG, von Jessen F, Sillesen H, Schroeder TV. Doppler spectral characteristics of infrainguinal vein bypasses. Euro Vasc Surg 1993;7: 610-5.

26. Papanicolaou G, Beach KW, Zierler RE, Strandness DE. Systolic flow limitation in stenotic lower-extremity vein grafts. J Vasc Surg 1996;23: 394-400.

27. Kleinstreuer C, Longest PW. Particle-hemodynamics analyses of end-to-side anastomoses: a computational comparison study. In: Tura A, editor. Vascular grafts: experiment and modeling. Ashurst, UK: WIT Press, 2003.

28. Cokelet GR. The rheology and tube flow of blood. In: Skalak R, Chien S, editors. Handbook of bioengineering. New York, NY: McGraw-Hill, 1987:14.1-17.

29. Buchanan JR, Kleinstreuer C. Simulation of particle hemodynamics in a partially occluded artery segment with implications to the initiation of microemboli and secondary stenoses. J Biomech Eng 1998;120:446-54.

30. Longest PW, Kleinstreuer C, Buchanan JR. Efficient computation of micron-particle dynamics including wall effects. Comp Fluids. Accepted for publication.

31. Longest PW, Kleinstreuer C, Buchanan JR. A new near-wall residence time model applied to three arterio-venous graft end-to-side anastomoses. Comput Methods Biomech Biomed Engin 2001;4:379-97.

32. Aarts PAMM, Steendijk P, Sixma JJ, Heethaar RM. Fluid shear as a possible mechanism for platelet diffusivity in flowing blood. J Biomech 1986;19:799-805.

33. Longest PW, Kleinstreuer C, Truskey GA, Buchanan JR. Relation between near-wall residence times of monocytes and early lesion growth in the rabbit aorto-celiac junction. Ann Biomed Eng 2003;31:53-64.

34. Goldsmith HL, Frojmovic MM, Braovac S, McIntosh F, Wong T. Adenosine diphosphate–induced aggregation of human platelets in flow through tubes. III: Shear and extrinsic fibrinogen-dependent effects. Thromb Haemost 1994;71:78-90.

35. Hellums JD. 1993 Whitaker Lecture. Biorheology in thrombosis research. Ann Biomed Eng 1994;22:445-55.

36. Pearson JD. Endothelial cell function and thrombosis. Baillieres Clin Haematol 1994;7:441-52.

37. Grabowski EF, Reininger AJ, Petteruti PG, Tsukurov O, Orkin RW. Shear stress decreases endothelial cell tissue factor activity by augmenting secretion of tissue factor pathway inhibitor. Arterioscler Thromb Vasc Biol 2001;21:157-62.

38. Harrison DG, Sayegh H, Ohara Y, Inoue N, Venema RC. Regulation of expression of the endothelial cell nitric oxide synthase. Clin Exp Pharmacol Physiol 1996;23:251-5.

39. Longest PW, Kleinstreuer C. Numerical simulation of wall shear stress conditions and platelet localization in realistic end-to-side arterial anastomoses. ASME J Biomech Eng 2003. In press.

40. Sharefkin JB, Diamond SL, Eskin SG, McIntire LV, Diefenbach CW. Fluid flow decreases preproendothelin mRNA levels and suppresses endothelin-1 peptide release in cultured human endothelial cells. J Vasc Surg 1991;14:1-9.

41. Helmke BP, Davies PF. The cytoskeleton under external fluid mechanical forces: hemodynamic forces acting on the endothelium. Ann Biomed Eng 2002;30:284-96.

42. Nagel T, Resnick N, Dewey CF, Gimbrone MA. Vascular endothelial cells respond to spatial gradients in fluid shear stress by enhanced activation of transcription factors. Vasc Biol 1999;19:1825-34.

43. Tardy Y, Resnick N, Nagel T, Gimbrone MA, Dewey CF. Shear stress gradients remodel endothelial monolayers in vitro via a cell proliferation-migration-loss cycle. Arterioscler Thromb Vasc Biol 1997;17: 3102-6.

44. Vorp DA. Computational biomechanics to guide and interpret vascular biology experiments. Presented at the Fourteenth US National Congress on Theoretic and Applied Mechanics; 2002; Blacksburg, Va.

45. Liu SQ. Biomechanical basis of vascular tissue engineering. Crit Rev Biomed Eng 1999;27(1 and 2):75-148.

46. Savage B, Saldivar E, Ruggeri ZM. Initiation of platelet adhesion by arrest onto fibrinogen or translocation on von Willebrand factor. Cell 1996;84:289-97.

47. Leu HJ, Feigl W, Susani M, Odermatt B. Differentiation of mononuclear cells into macrophages, fibroblasts, and endothelial cells in thrombus organization. Exp Cell Biol 1988;56:201-10.

48. Sloope GD, Fallon KB, Zieske AW. Atherosclerotic plaque-like lesions in synthetic arteriovenous grafts: implications for atherogenesis. Atherosclerosis 2002;160:133-9.

49. Longest PW, Kleinstreuer C. Computational haemodynamics analysis and comparison study of arterio-venous grafts. J Med Eng Tech 2000; 24:102-10.